Journal of Solid State Chemistry **154,** 488–497 (2000)
doi:10.1006/jssc.2000.8869, available online at http://www.idealibrary.com on IDEAL®

Synthesis and Study of Hg-Based 1222-Type Superconducting Cuprates (Hg, *M*)Sr_2(*Ln*, Ce)$_2Cu_2O_z$

E. Kandyel,[1,2] A. Yamamoto, J. G. Wen,[3] and S. Tajima

Superconductivity Research Laboratory, ISTEC, 10–13 Shinonome 1-Chome, Koto-ku, Tokyo 135-0062, Japan

Received April 7, 2000; in revised form June 8, 2000; accepted July 13, 2000; published online September 30, 2000

A novel series of "1222-type" copper oxides described by the formula (Hg, *M*)Sr_2(*Ln*, Ce)$_2Cu_2O_z$ (*M* = Ti, V, Cr, Mo, W, Re; and *Ln* = Sm, Eu, Gd, Dy, Ho, Er) have been synthesized under high pressure. The structure was determined by combination of X-ray powder diffraction, electron diffraction and high-resolution electron microscopy measurements. The materials are isostructural with (Pb, Cu)-1222, crystallizing in a tetragonal unit cell, space group *I4/mmm*. The compounds adopt the 1222-type structure with an intergrowth of three types of layers: oxygen-deficient perovskite (CuO_5 pyramidal layers), double fluorite-type layers, and double rock-salt layers. A correlation between lattice parameters and effective ionic radii of the (*Ln*, Ce) site is determined for ($Hg_{0.75}W_{0.25}$)Sr_2(*Ln*$_{1.5}$Ce$_{0.5}$)Cu_2O_z, *Ln* = Sm–Er. Except for Cr-containing compound, bulk superconductivity is observed in all the synthesized compounds. The value of T_c is related to both the effective ionic radius of the (*Ln*, Ce) site and the valence of the *M*-element. Among these compounds, the sample with nominal composition of ($Hg_{0.75}W_{0.25}$)Sr_2($Gd_{1.5}Ce_{0.5}$)Cu_2O_z recorded the highest T_c up to 75 K. © 2000 Academic Press

Key Words: **high-T_c superconductors; (Hg, *M*)-1222; high-pressure synthesis; X-ray powder diffraction; magnetic susceptibility.**

INTRODUCTION

The superconducting family of the homologous series $HgBa_2Ca_{n-1}Cu_nO_{2n+2+\delta}$ (Hg-12($n-1$)n) remains the subject of intensive research activity since its discovery (1), fueled by the very high critical temperatures observed at 97(2), 127(3), 135(4), and 127 K (5) for the $n = 1$, 2, 3, and 4 members, respectively. One of the interesting properties of this family is that many transition elements can occupy the mercury site in spite of their different valences and much smaller ion sizes than those of Hg (6–9). Although such substitution changes both the carrier doping state and the local crystal structure, the original high T_c has been kept higher than 130 K for $n = 3$, Hg-1223. Moreover, partial substitution of Hg by such high-valence transition elements is—up to now—the only way of stabilizing the Ba-free $HgSr_2Ca_{n-1}Cu_nO_{2n+2+\delta}$ series. For $HgSr_2CuO_z$ partial substitution of Cr, Mo, and Re for Hg (10, 11) was necessary for structural stabilization, and T_c was lower than 75 K. In the case of the (Hg, *M*)$Sr_2CaCu_2O_z$, an additional substitution of a rare-earth element for Ca is required for synthesis under ambient pressure (11–20). T_c of these (Hg, *M*)-1212 compounds was approximately 100 K.

As to the (Hg, *M*)-1222 with fluorite-type block layers, a series of compounds (Hg, *M*)$Sr_2Pr_2Cu_2O_z$ (*M* = Pr, Pb, Bi, Tl) were synthesized by a solid state reaction in sealed quartz tubes (21). However, these cuprates were nonsuperconducting even after annealing in oxygen pressure up to 100 bar. Although superconductivity at 38 K was reported for (Hg, Pb)Sr_2(Gd, Ce)$_2Cu_2O_z$, which was synthesized by the sol–gel method after annealing in 10 bar of oxygen pressure (22), it is a puzzle why the T_c value is low, compared with the other Hg-based cuprate superconductors.

The first superconductor containing fluorite-type block layers is (Nd, Sr)(Nd, Ce)CuO_4 (T*-214), discovered by Akimitsu *et al.* (23, 24). After their discovery, superconductors with fluorite-type block layers, such as (Nd, Ce)$_2CuO_4$ (T′-214) (25), (*Ln*, Ce)$_2$(Ba, *Ln*)$_2Cu_3O_{10}$ (Cu-1222, *Ln* = rare-earth elements) (26, 27), and (Pb, Cu) (Sr, *Ln*)$_2$(*Ln*′, Ce)$_2Cu_2O_z$ ((Pb, Cu)-1222, *Ln*, *Ln*′ = rare-earth elements) (28–30), were prepared. The maximum T_c values of these systems are 35 K for T*-214, 24 K for T′-214, 43 K for Cu-1222, and 35 K for (Pb, Cu)-1222. It is note worthy that the T_cs of 1222 superconductors reported previously are below 45 K. The low T_c may be essential for the 1222-type superconductors. However, optimization of synthesis and annealing conditions has not been performed for almost all 1222 superconductors and further studies are needed to determine the highest T_c value for this type of compound.

[1]To whom correspondence should be addressed. Fax: (0081)3-3536-5717. E-mail: kandyel@istec.or.jp.

[2]Permanent address: Chemistry Department, Faculty of Science, Tanta University, Tanta, Egypt.

[3]Present address: Physics Department, Boston College, 140 Commonwealth Ave., Chestnut Hill, MA 02167.

0022-4596/00 $35.00

The purpose of this study was to find new superconductors containing fluorite-type block layers for enhancing T_c of 1222 superconductors. In the present paper, we report on high-pressure synthesis and superconductivity of new "1222-type" compounds, (Hg, M)$Sr_2(Ln, Ce)_2Cu_2O_z$, M = Ti, V, Cr, Mo, W, Re, and Ln = rare-earth elements. The highest T_c value observed was 75 K, which is the highest among the 1222-type superconductors containing double fluorite-type block layers. On the basis of the crystal structure results determined by X-ray powder diffraction supported with electron diffraction and high-resolution transmission microscopy studies, a correlation between T_c and an effective ionic radius of rare-earth elements is discussed.

EXPERIMENTAL

Samples with (Hg, M)-1222 type were prepared in a multistep process. First, two precursors, $Sr_2(Gd_{2-y}Ce_y)Cu_2O_z$, $y = 0$–1, and $Sr_2(Ln_{1.5}Ce_{0.5})Cu_2O_z$, were made by mixing $SrCO_3$, CeO_2, Ln_2O_{30} (Ln = La–Yb) and CuO with purity of 99.9% or better in appropriate molar ratios. Each mixture was finely ground under acetone in an agate mortar with a pestle. The well mixed powder was pressed into tablets of 6 mm diameter and 4 mm thickness. The tablet was initially heated in flowing O_2 from room temperature to 900°C, maintained at that temperature for 24 h, and then furnace-cooled to room temperature. It was then reground, repelletized, and calcined at 950°C for 48 h under O_2 flow and slowly cooled to room temperature.

The individual calcined tablets of the precursors were then transferred to a dry box (vacuum atmosphere) and a pellet of each composition was separately ground and mixed with HgO and TiO_2, V_2O_5, Cr_2O_3, MoO_3, WO_3, or ReO_3 according to the nominal compositions,

$(Hg_{1-x}W_x)Sr_2(Gd_{2-y}Ce_y)Cu_2O_z$, ($0.0 \le x \le 0.5$, $0.0 \le y \le 1.0$)
$(Hg_{0.75}W_{0.25})Sr_2(Ln_{1.5}Ce_{0.5})Cu_2O_z$, ($Ln$ = La, Nd, Sm, Eu, Gd, Dy, Ho, Er, Tm, and Yb)
$(Hg_{0.75}M_{0.25})Sr_2(Gd_{1.5}Ce_{0.5})Cu_2O_z$, ($M$ = Ti, V, Cr, Mo, W, and Re),

thoroughly mixed, pressed into pellets, and sealed in an Au tube for high-pressure, high-temperature synthesis. High-pressure was applied to the pellet using a cubic-anvil-type apparatus. Pyrophillite was used as the pressure transfer medium. A graphite tube was used as a heater. First, pressure was gradually increased up to 2 GPa over a time span of 1 h, and then heat treatment was performed at 1100°C for 2 h. Next, the sample was quenched by reducing the electrical power to zero, and finally pressure was relaxed in 1 h.

The crystal structure of the samples were examined by a powder X-ray diffraction (XRD) using Ni-filtered Cu$K\alpha$ radiation. Step-scanned data were collected at 0.02° intervals for 5 s over a 2θ range from 3 to 120°. The intensity data were refined by a Rietveld analysis computer program RIETAN provided by Izumi (31). Electron diffraction (ED) and high-resolution transmission electron microscopy (HRTEM) were performed using a JEOL-4000EX instrument operating at 400 kV. Specimens for ED and HRTEM examination were ground in an agate mortar with acetone for a few minutes, and the powder was transferred to a copper grid, upon which a holly carbon film had been deposited. The compositional analysis of crystal grains were carried out using an energy-dispersive X-ray analyzer attached to a TEM (TEM-EDX).

Superconductivity transitions were determined from measurements of both electrical resistivity and Meissner diamagnetic susceptibility as a function of temperature. Electrical resistivity measurements were performed by a standard four-probe DC method. The magnetic susceptibility was measured between 100 and 5 K in the "field-cooling" mode, using a superconducting quantum interference device (SQUID) magnetometer. The field was kept at 20 Oe throughout the measurement. The measured magnetic moment (emu) was divided by the weight of the sample to yield mass magnetization, χ (emu/g) which was plotted as a function of temperature.

RESULTS AND DISCUSSION

$(Hg_{1-x}W_x)Sr_2(Ln_{2-y}Ce_y)Cu_2O_z$

In the first stage of high-pressure synthesis, we concentrated our effort on the W-containing materials $(Hg_{1-x}W_x)Sr_2(Ln_{2-y}Ce_y)Cu_2O_z$ to investigate the optimum composition. Three examples of samples with various nominal compositions were prepared to obtain single-phase materials with the (Hg, W)-1222 structure and examined by XRD analysis.

Example 1. For Ln = Gd, the x value was fixed at 0.25 and the y value was varied ($0 \le y \le 1$) to examine a solid solution range of Gd and Ce. The samples in the $0.4 \le y \le 0.7$ range are primarily in a single phase. The samples of $y \ge 0.8$ contain CeO_2 as impurity and those of $y \le 0.3$ contain the (Hg, W)-1212 phase.

Example 2. For Ln = Gd, y was fixed at $y = 0.5$ and x was varied ($0 \le x \le 0.5$) to examine a suitable W content. The XRD analysis revealed that the samples with nominal composition of $x \le 0.15$ and $x \ge 0.35$ were multiphases and no evidence for the 1222 phase was detected. However, the samples with $x = 0.2 - 0.3$ had a nearly single phase of (Hg, W)-1222 structure. This indicates that the substitution of a certain amount of W^{6+} for Hg^{2+} is effective to the formation of the (Hg, W)-1222 phase. Such results were also reported for (Hg, W)Sr_2(Sr, La)$_{n-1}Cu_nO_z$, $n = 1$, 2 (17).

Example 3. The rare-earth elements in $(Hg_{0.75}W_{0.25})Sr_2(Ln_{1.5}Ce_{0.5})Cu_2O_z$ were varied as Ln = La, Nd, Sm, Eu, Gd, Dy, Ho, Er, Tm, and Yb to examine suitable ionic radii of the rare earth for phase stability. Single-phase materials or those with only a small amount of CeO_2 were formed for the samples of Ln = Sm, Eu, Gd, Dy, Ho, and Er. However, for La, Nd, Tm, and Yb, the Hg-1222 phase was not obtained. We suggest that the formation of (Hg, W)-1222 needs a suitable ionic radius of Ln^{3+}, the radii of La^{3+} and Nd^{3+} being too large and those of Tm^{3+} and Yb^{3+} too small. Therefore, the (Hg, W)-1222 structure containing these ions cannot be formed under the same conditions as those for the successful rare-earth elements.

The XRD patterns for the samples having nominal compositions $(Hg_{0.75}W_{0.25})Sr_2(Ln_{1.5}Ce_{0.5})Cu_2O_z$ (Ln = Sm and Er) are shown in Fig. 1. The patterns are similar to that of the (Pb, Cu)-1222 phase and all the diffraction peaks can be indexed based on a tetragonal body-centered lattice. The space group of the highest symmetry expected from the extinction rule is $I4/mmm$ (No. 139). Diffraction peaks attributed to the 1222 phase showed a shift in 2θ position for the different samples, as would be expected from replacing different sized rare-earth ions on the rare-earth site. The lattice parameters are: $a = 3.8327(7)$, $c = 29.150(6)$ Å for Ln = Gd sample, which are close to those of (Pb, Cu)-1222 ($a = 3.8379$, $c = 29.0116$ Å) (30).

Numerous crystals in the sample with nominal composition $(Hg_{0.75}W_{0.25})Sr_2(Gd_{1.5}Ce_{0.5})Cu_2O_z$ were studied by ED, reconstructing the reciprocal space, and checking the purity of the sample. This study gave evidence for the presence of small grains of unreacted CeO_2 in the phase, but in a very small amount (about 2 grains per each 50 characterized grains). The majority of the crystals exhibit a tetragonal cell with $a \sim 3.83$ Å and $c \sim 29$ Å; hkl reflections with $h + k + l$ = odd are systematically absent and the condition limiting the reflections are hkl, $h + k + l = 2n$, which involve a I-type space group.

The results of the TEM-EDX compositional analysis are shown in Table 1 for several grains in the sample with nominal composition $(Hg_{0.75}W_{0.25})Sr_2(Gd_{1.5}Ce_{0.5})Cu_2O_z$. No significant dispersion of chemical composition was observed among the grains and the average composition is very close to the nominal one, within the experimental error. The average cation ratio was Hg:W:Sr:Gd:Ce:Cu $\approx$ 0.73:0.27:2.0:1.52:0.48:2.0. The ratios of W/Hg and Ce/Gd are 0.36 and 0.31, respectively, whereas, both Sr and Cu contents are almost 2.

Typical [001] and [010] electron diffraction patterns are given in Figs. 2a and 2b. It can be seen that the reflections are very sharp and no streaks are observed along the c-axis. This observation suggests a good ordering of the layer stacking along the c-axis; this was checked by recording the corresponding bright field images; the periodicity of the fringes, 14.5 Å spaced, is very regular, as shown in Fig. 2c, suggesting a statistical distribution of the cations (Hg and W) within the rock salt layers $(Hg_{0.75}W_{0.25}O_{1-\delta})$. There is no kind of superstructure or defect as seen in (Hg, Pr)-1222 materials (21). In (Hg, Pr)-1222 compound $(Hg_{0.4}Pr_{0.6})Sr_2(Pr_{1.7}Sr_{0.3})Cu_2O_z$, an ordering of the cations in the $(Hg_{0.4}Pr_{0.6}O_{1-\delta})$ plane was observed and it was very defective. Three types of extended defects have been reported: (i) Replacement of a single $(Hg_{1-x}Pr_xO_{1-\delta})$ layer by a double $(Hg_{1-x}Pr_xO_{1-\delta})_2$ layer, forming locally a 2222-type structure. (ii) A double Pr layer is locally eliminated; leading to the formation of the (Hg, Pr)-1201 structure. (iii) A double fluorite layer is replaced by a slab of six layers in the fluorite configuration.

Figure 3 shows the refined tetragonal lattice parameters, a and c, and the unit cell volume as a function of the effective ionic radius for $(Ln_{1.5}Ce_{0.5})$ site of $(Hg_{0.75}W_{0.25})Sr_2(Ln_{1.5}Ce_{0.5})Cu_2O_z$ with Ln = Sm, Eu, Gd, Dy, Ho, and Er.

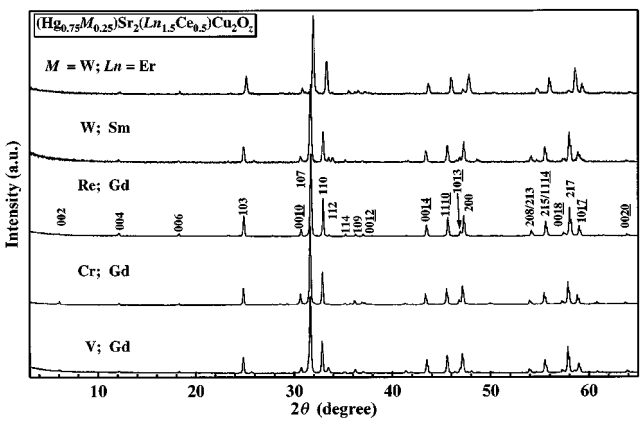

FIG. 1. XRD patterns for the samples with nominal composition $(Hg_{0.75}M_{0.25})Sr_2(Ln_{1.5}Ce_{0.5})Cu_2O_z$ synthesized under 2 GPa at 1100°C. The indexed lines are attributed to (Hg, M)-1222 with a tetragonal cell.

TABLE 1

Chemical Analysis of Cationic Ratio by TEM-EDX for the Sample with Nominal Composition $(Hg_{0.75}W_{0.25})Sr_2(Gd_{1.5}Ce_{0.5})Cu_2O_z$

Sample No.	Hg	W	Sr	Gd	Ce	Cu
	11.0	3.7	29.2	22.6	6.9	26.6
	10.6	2.7	26.7	21.4	6.1	32.5
	11.3	3.8	31.5	18.9	7.5	27.0
	9.1	4.9	28.2	20.8	8.6	26.4
	10.6	2.7	26.2	24.3	5.7	30.5
	8.9	4.2	27.2	21.9	6.6	31.2
	9.6	5.0	32.0	20.7	5.2	27.5
	12.9	3.0	27.0	23.0	6.3	27.8
Average	10.50	3.78	28.51	21.71	6.81	28.69
Nominal	10.71	3.57	28.57	21.43	7.14	28.57

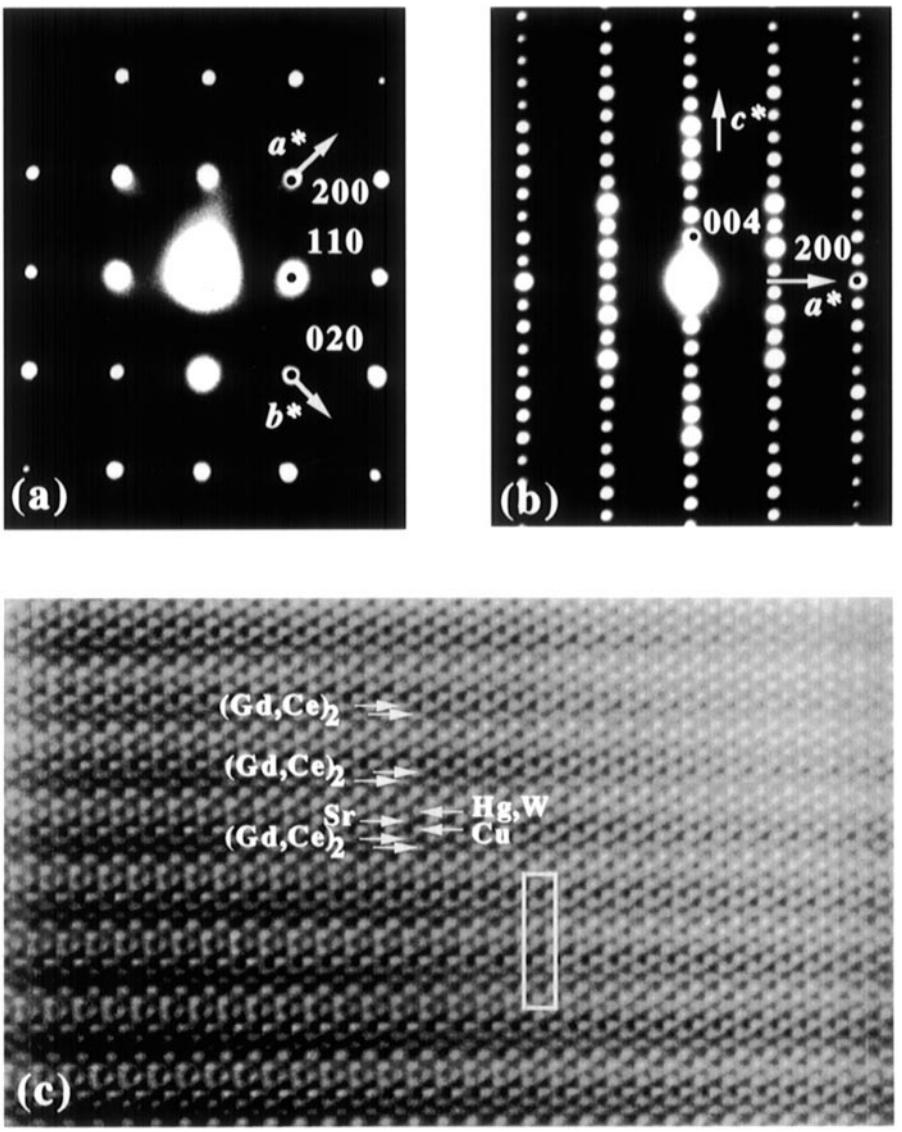

FIG. 2. The *hk*0 (a) and *h*0*l* (b) electron diffraction patterns and a lattice image projected along [010] (c) for the $(Hg_{0.75}W_{0.25})Sr_2(Gd_{1.5}Ce_{0.5})Cu_2O_z$ sample.

Both *a* and *c*, as well as the volume of a unit cell, scale up as expected with increasing effective ionic radius of $(Ln_{1.5}Ce_{0.5})$ site. This correlation suggests that the rare-earth ions are successfully incorporated in the (Hg, W)-1222 phase.

Figures 4a and 4b schematically show idealized crystallographic structures of (Hg, *M*)-1222, (Hg, *M*)Sr_2(*Ln*, Ce)$_2Cu_2O_z$, and (Hg, *M*)-1222, (Hg, *M*)Sr_2(*Ln*, Ca)Cu_2O_z, respectively. The (Hg, *M*)-1222 structure is derived from (Hg, *M*)-1212 by replacing the (*Ln*, Ca) layer with a fluorite structured (*Ln*, Ce)$_2O_2$ layer. In addition, the length of the unit cell in the *c* direction is doubled due to a glide plane introduced by the (*Ln*, Ce)$_2O_2$ layer. In the present structure refinement for the (Hg, *M*)-1222; $(Hg_{0.75}W_{0.25})Sr_2(Ln_{1.5}Ce_{0.5})Cu_2O_z$ (*Ln* = Sm, Eu, Gd, Dy, Ho, and Er), the initial structure model was that of the (Hg, *M*)-1222 phase, with additional double fluorite layers introduced between the CuO_2 sheets in the place of single fluorite layer. The space group of *I*4/*mmm* was employed for this model. As shown in Fig. 4a, there are four different crystallographic sites for the metal atoms in the (Hg, *M*)-1222 structure. We supposed that Sr^{2+} and Ce^{4+} occupied different crystallographic sites because of the large difference in their ionic radii (32). Since the *M′* and *M″* sites are folded by nine and eight oxygen atoms, respectively, the *M′* site is expected to be favorable for relatively large ions such as Sr^{2+} and the *M″* site for relatively small ions such as Ce^{4+} and Ln^{3+}.

Preliminary refined values for the Hg/W and *Ln*/Ce ratios agree well with those obtained from TEM-EDX analysis

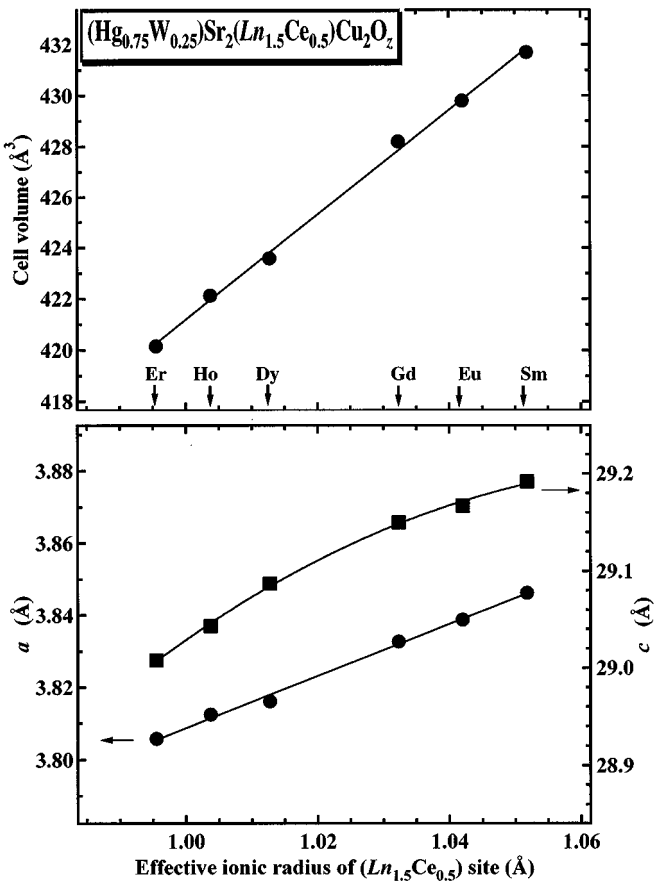

FIG. 3. Dependence of the tetragonal lattice parameters, a and c, and unit cell volume on the effective ionic radii, r, of the $(Ln_{1.5}Ce_{0.5})$ site in the composition $(Hg_{0.75}W_{0.25})Sr_2(Ln_{1.5}Ce_{0.5})Cu_2O_z$.

and were very close to those for the nominal compositions, and therefore, in the final refinements, these ratios were fixed at the nominal ones. Positional parameters and isotropic thermal parameters were successfully refined. The refinement went well except to meaningless negative values. The problems were solved by allowing the O(4) to occupy a split position (8*j*) and fixing the thermal parameter of O(3) (the selection of 0, 0.5, or 1 for *B*O(3) actually did not alter the agreement factors).

After successive refinements, the different agreement factors are minimized to the parameters given in Table 2. The good agreement between the observed and calculated XRD patterns, is shown for $Ln = Gd$, as an example, in Fig. 5, where the low R factors indicate that the assigned structure model is correct.

Bond distances and angles were calculated from the refinement results and some selected values are presented in Table 3. Some comments can be made using the results of the present XRD refinements.

(i) All the distances agree well with those observed in (Hg, *M*)-1212, (Pb, Cu)-1222 and other cuprate superconductors. (ii) The apical (Hg/W)–O distance (2.1–2.15 Å) is longer than that observed in pure mercury cuprates (1.95 Å). (iii) The (*Ln*, Ce)–O_8 cages are slightly elongated along the *c*-direction (O–O distances are 2.71 Å in the *ab* plane and 2.95 Å in the *ac* plane) and *Ln* and Ce are displaced from the center of their coordination polyhedron, as was observed in the XRD study of $(Hg_{0.3}Tl_{0.7})Sr_2Pr_2Cu_2O_z$ (21), which exhibits the double fluorite-type layers. (iv) The CuO_5 pyramids are characterized by four in-plane distances (1.90–1.92 Å) and one long apical distance (2.12–2.15 Å). (v) The CuO_2 planes showed the buckling characteristic of high-T_c oxide superconductors. The SrO planes showed a buckling similar to that of the CuO_2 planes with the displacement of the O(1) site from the SrO plane in the opposite direction of the displacement of the O(2) site from the nearest CuO_2 plane. These X-ray results should be compared with neutron diffraction data to clarify, with as much accuracy as possible, the oxygen coordinates and occupancies, which are of major interest for the superconducting properties.

Figures 6a and 6b show the temperature dependence of electrical resistivity for samples with nominal composition $(Hg_{0.75}W_{0.25})Sr_2(Ln_{1.5}Ce_{0.5})Cu_2O_z$, Ln = Sm, Eu, Gd, Dy, Ho, and Er. All the samples show a metallic behavior from room temperature down to superconducting transition onset at about 56, 65, 75, 71, 65, and 60 K, respectively. T_c zero is also observed for these samples at 34, 39, 48, 49, 42, and 36 K, respectively.

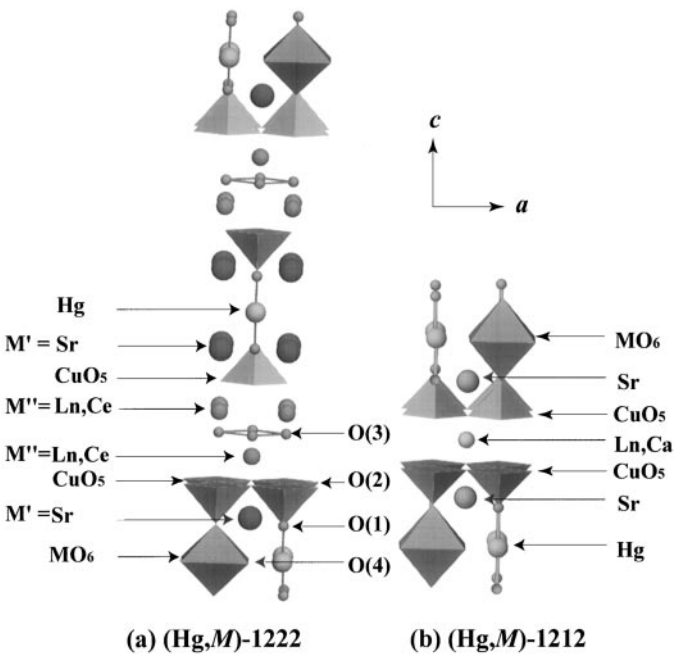

FIG. 4. Schematic structural models for (a) (Hg, *M*)-1222, (Hg, *M*)$Sr_2(Ln, Ce)_2Cu_2O_z$ and (b) (Hg, *M*)-1212, (Hg, *M*)$Sr_2(Ln, Ca)Cu_2O_z$ phases.

TABLE 2
Part of the Structural Parameters Obtained by the Rietveld Analysis of the XRD Data and T_c for the $(Hg_{0.75}W_{0.25})Sr_2(Ln_{1.5}Ce_{0.5})Cu_2O_z$ Samples, Space Group *I*4/*mmm*

		Ln					
		Sm	Eu	Gd	Dy	Ho	Er
T_c (K)		56	65	75	71	64	60
a (Å)		3.8462(7)	3.8386(7)	3.8327(7)	3.8161(1)	3.8124(1)	3.8058(2)
c (Å)		29.182(5)	29.167(7)	29.150(6)	29.087(1)	29.043(1)	29.008(1)
R_I		5.75	5.17	4.27	4.25	5.92	5.70
R_P		6.63	6.67	6.25	6.40	6.55	6.85
R_{WP}		9.01	8.88	8.14	8.62	8.20	9.53
R_e		4.25	4.09	4.25	4.38	4.43	4.30
(Hg, W)	2a (0, 0, 0)						
	B (Å^2)	0.66(9)	0.2(2)	0.44(3)	0.3(2)	0.53(1)	0.4(1)
Sr	4e (0, 0, z)						
	z	0.0844(4)	0.0846(1)	0.0847(1)	0.0848(3)	0.0850(3)	0.0851(5)
	B (Å^2)	0.2(2)	0.3(2)	0.17(4)	0.3(2)	0.5(2)	0.4(4)
(*Ln*, Ce)	4e (0, 0, z)						
	z	0.2067(3)	0.2070(2)	0.2072(5)	0.2076(3)	0.2079(3)	0.2079(3)
	B (Å^2)	0.28(6)	0.4(2)	0.25(3)	0.3(2)	0.38(8)	0.3(1)
Cu	4e (0, 0, z)						
	z	0.1445(8)	0.1453(4)	0.146(1)	0.1464(7)	0.1473(6)	0.147(1)
	B (Å^2)	0.7(3)	0.47(5)	0.26(5)	0.2(2)	0.6(3)	0.35(2)
O(1)	4e (0, 0, z)						
	z	0.072(2)	0.073(4)	0.072(2)	0.074(2)	0.073(2)	0.073(3)
	B (Å^2)	2.2(3)	1.9(3)	2.0(4)	1.7(2)	2.1(5)	1.8(3)
O(2)	8g (0, 0.5, z)						
	z	0.146(2)	0.148(3)	0.148(4)	0.149(2)	0.150(2)	0.149(2)
	B (Å^2)	1.9(3)	1.8(6)	2.0(5)	2.3(7)	1.9(3)	2.3(3)
O(3)	4d (0, 0.5, 0.25)						
	B (Å^2)	0.5	0.5	0.5	0.5	0.5	0.5
O(4)	8j (x, 0.5, 0)						
	x	0.41(6)	0.41(3)	0.409(6)	0.35(4)	0.36(4)	0.35(5)
	g	0.25	0.25	0.25	0.25	0.25	0.25
	B (Å^2)	1.0(6)	1.8(2)	1.3(2)	1.3(3)	1.1(5)	1.5(5)

Figures 6c and 6d show the temperature dependence of the magnetic susceptibility for the same samples measured under field-cooling conditions with $H = 20$ Oe. Only one-step transition is observed for each sample, indicating the presence of only one superconducting phase in full agreement with the results of XRD and electron diffraction. The onset T_c is 56, 65, 75, 71, 64, and 60 K for samples with Ln = Sm, Eu, Gd, Dy, Ho, and Er, respectively, which agree well with the onset T_cs determined by resistivity measurements in Figs. 6a and 6b. The superconducting volume fractions estimated from the susceptibility at 5 K and crystal density are 25, 24, 21, 22, 14, and 32% for Ln = Sm, Eu, Gd, Dy, Ho, and Er, respectively. This result indicates that the observed superconductivity is indeed a bulk nature.

T_cs of the samples are summarized in Fig. 7a as a function of the effective ionic radius of $(Ln_{1.5}Ce_{0.5})$ site, r. T_c increases proportionally to r in the small r region to a maximum value of 75 K at $r = 1.03$ Å for Ln = Gd, and decreases again for $r > 1.03$ Å. Thus, a dependence of T_c on r exhibits a cupola-shaped behavior. The possible explanation for this phenomenon might be an insufficient and extra carrier concentration for the samples having rare-earth elements with smaller (Dy, Ho, Er) and larger (Eu, Sm) r values, respectively. The carrier concentration and hence, T_c in the $(Hg_{0.75}W_{0.25})Sr_2(Ln_{1.5}Ce_{0.5})Cu_2O_z$ system, may thus be tuned from the underdoped to overdoped regime as the r value is increased. Wada *et al.* (27) and Sakai *et al.* (30) reported that T_cs of the Cu-1222 and (Pb, Cu)-1222 phases, which had a similar structure to the present case, were strongly dependent not only on the oxygen content but also on the thickness of the double fluorite layers separating two neighboring CuO_2 sheets. Wada *et al.* (33) also reported that the (Pb, Cu)-1232 phase, which structurally contained thicker fluorite-blocks (triple fluorite layers), was nonsuperconducting. From these results, we expect that the variation in T_c of the present (Hg, W)-1222 compounds is attributed

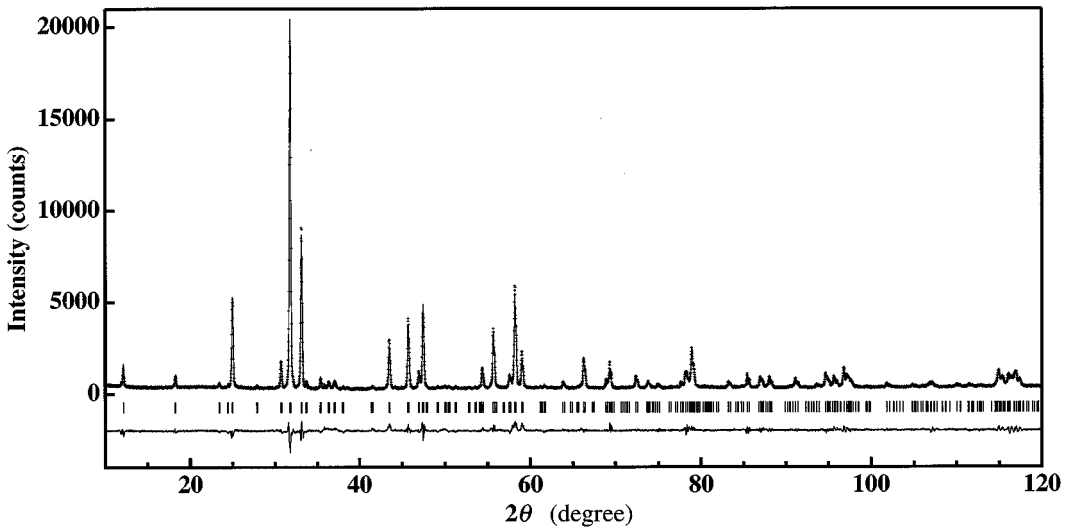

FIG. 5. Measured (crossed line) and refined (solid line) XRD patterns from the Rietveld analysis for the $(Hg_{0.75}W_{0.25})Sr_2(Gd_{1.5}Ce_{0.5})Cu_2O_z$ sample.

to the change in hole concentration and also to the change in thickness of the fluorite block.

It is evident from Figs. 3 and 7a that both lattice parameters and T_cs in (Hg, W)-1222 system are correlated by the size of the *Ln* ion. Similar correlation of lattice parameters and/or T_c with ionic radii of the rare-earth elements has also been observed in (Pb, Cu)-1222 system (30) prepared by heat treatment in 90 atm oxygen, but the reported dependence of T_c on the size of rare-earth element is slightly different from our results. Sakai *et al.* (30) observed that T_c increases linearly as the size of a rare-earth ion increases from Ho to Gd and then remains constant for larger ions up to Sm. This difference may come from the different methods of preparation, where samples of (Hg, W)-1222 prepared under 2 GPa have more oxygen content, and hence, more hole concentration, than (Pb, Cu)-1222 annealed in 90 atm of O_2.

$(Hg_{0.75}M_{0.25})Sr_2(Gd_{1.5}Ce_{0.5})Cu_2O_z$

Next, we investigated stabilization of (Hg, *M*)-1222 phase by using other high-valence transition metals. Various transition metals with different valences such as Ti^{4+}, V^{5+}, Cr^{6+}, Mo^{6+}, and Re^{7+} are tested to examine the effect of their valence on the superconductivity. The XRD patterns of the high-pressure products of $(Hg_{0.75}M_{0.25})Sr_2(Gd_{1.5}Ce_{0.5})Cu_2O_z$ samples with $M = V$, Cr, and Re are

TABLE 3
Selected Bond Distances (Å) and Angles (Degree) for the $(Hg_{0.75}W_{0.25})Sr_2(Ln_{1.5}Ce_{0.5})Cu_2O_z$ Samples

		Ln					
Bond	*N*	Sm	Eu	Gd	Dy	Ho	Er
Hg/W–O(1)	2	2.0968(3)	2.1033(3)	2.0958(6)	2.1499(1)	2.1307(3)	2.1282(4)
Hg/W–O(4)	$\frac{8}{4}$	2.4980(5)	2.4835(2)	2.4773(3)	2.3388(6)	2.3525(5)	2.3345(5)
Hg/W–O(4)	$\frac{8}{4}$	2.9614(2)	3.0967(2)	2.9652(1)	3.1286(3)	3.0913(3)	3.1048(2)
Sr–O(1)	4	2.7442(2)	2.7410(3)	2.7354(3)	2.7228(2)	2.7169(4)	2.7127(5)
Sr–O(2)	4	2.6305(7)	2.6508(4)	2.6739(3)	2.6733(1)	2.6804(2)	2.6525(5)
Sr–O(4)	$\frac{4}{4}$	2.4843(6)	2.4993(5)	2.4888(5)	2.5350(2)	2.5250(2)	2.5307(3)
Ln/Ce–O(2)	4	2.6162(1)	2.5892(3)	2.5573(2)	2.5663(4)	2.5434(2)	2.5598(3)
Ln/Ce–O(3)	4	2.3015(5)	2.2973(3)	2.2812(5)	2.2757(5)	2.2648(2)	2.2614(3)
Cu–O(1)	1	2.1189(2)	2.1365(5)	2.1478(6)	2.1459(3)	2.1389(6)	2.1316(2)
Cu–O(2)	4	1.9236(2)	1.9197(3)	1.9184(2)	1.9133(1)	1.9077(1)	1.9038(3)
O(2)–Cu–O(2)		174.91	175.70	176.12	175.58	175.37	175.29
O(1)–Sr–O(1)		169.03	165.73	168.46	167.17	167.34	166.47

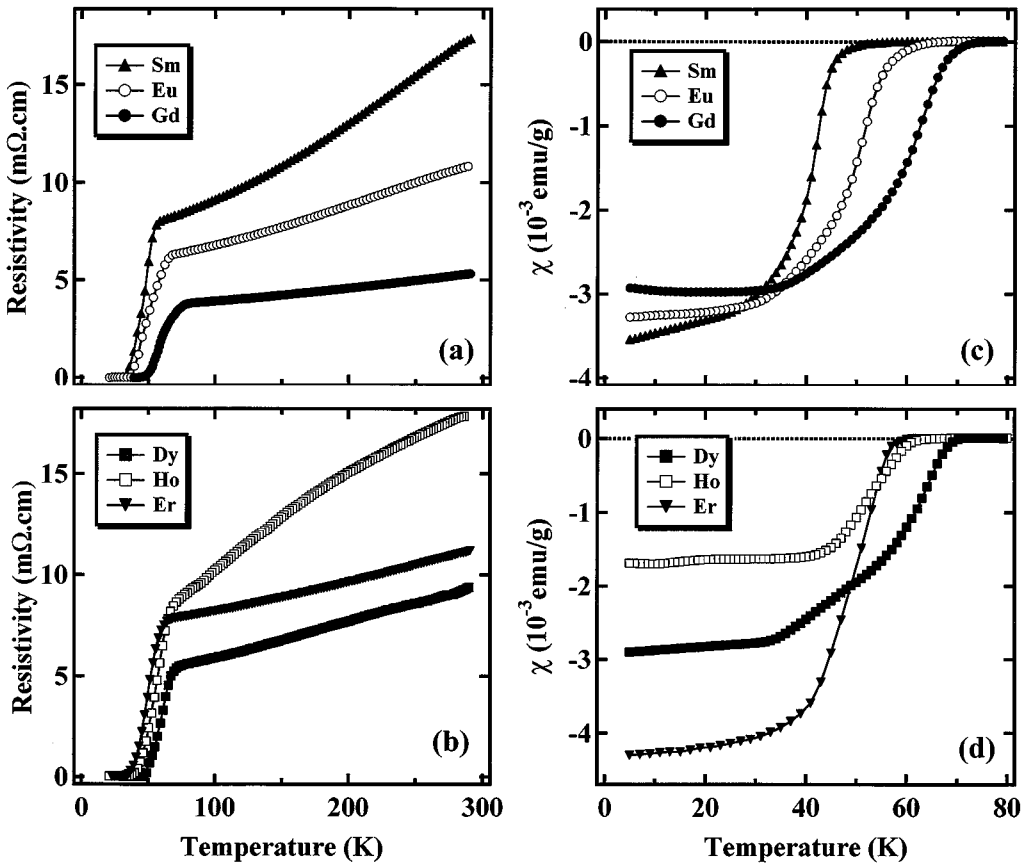

FIG. 6. Temperature dependencies of (a and b) electrical resistivity and (c and d) magnetic susceptibility for the $(Hg_{0.75}W_{0.25})Sr_2(Ln_{1.5}Ce_{0.5})Cu_2O_z$ samples. The magnetic susceptibility is measured in field-cooling conditions in an external field of 20 Oe.

shown in Fig. 1 and Table 4 lists their structural and superconducting properties. The phase identification results for these samples indicate that they are (Hg, *M*)-1222 of single phase or with a small amount of unknown impurity phases.

Notably, the *c* parameters of the Cr and V-containing (Hg, *M*)-1222 samples are observed to be significantly shorter than those of the Ti-, Mo-, W-, and Re-containing samples. According to the structural analysis for the (Hg, Cr)$A_2CuO_{4+\delta}$ phase, A = Sr or Ba, chromium adopts tetrahedral coordination, forming CrO_4 units with two oxygen atoms apical of the CuO_5 pyramids and two others located in the (Hg, Cr) plane (34, 35). On the other hand, Ti, Mo, W, and Re adopt octahedral coordination forming MO_6 units with two oxygen atoms apical of the CuO_5 and four other located in the (Hg, *M*) plane of (Hg, *M*)$Sr_2(Ca, Y)_{n-1}Cu_nO_z$, $n = 2$, 3 phases (20, 36). Similar situations may occur in the present (Hg, *M*)-1222 phases. As the CrO_4 and VO_4 tetrahedrons are small enough compared with TiO_6, MoO_6, WO_6, and ReO_6 octahedrons, the *c* parameters of the Cr- and V-containing samples can be shorter.

In Fig. 8 we show the temperature dependence of the magnetization of $(Hg_{0.75}M_{0.25})Sr_2(Gd_{1.5}Ce_{0.5})Cu_2O_z$ samples with M = Ti, V, Cr, Mo, W, and Re. It can be seen in Fig. 8a that, except the Cr-containing sample, all samples exhibit bulk superconductivity with volume fractions of 20, 11, 21, 21, and 15% for M = Ti, V, Mo, W, and Re, respectively. Figure 7b shows the T_cs vs the valences of the M elements. It roughly indicates that T_c increases with increasing valences of the M elements. With increasing valence of the M elements, the coordination also increases and thus more oxygen is introduced into the HgO_δ planes, resulting in higher hole concentration and higher T_c. The results of Re- and Cr-containing samples deviate from this behavior. The diamagnetic signal of the Re-containing sample appeared at 50 K which can be further enhanced up to 70 K, when 10% by weight of $LiClO_4$ was used as an oxidant during the synthesis process (Fig. 8b). Moreover, using ReO_2 as a starting source for Re, T_c decreases down to 39 K. These results suggest that the Re-containing sample in Fig. 8a is in the underdoped regime and an increase in the oxygen content is needed to optimize its T_c. On the other hand, Cr-containing samples did not show superconductivity even with using an oxidizing agent, $LiClO_4$, during the synthesis process. It should be mentioned that the (Hg,

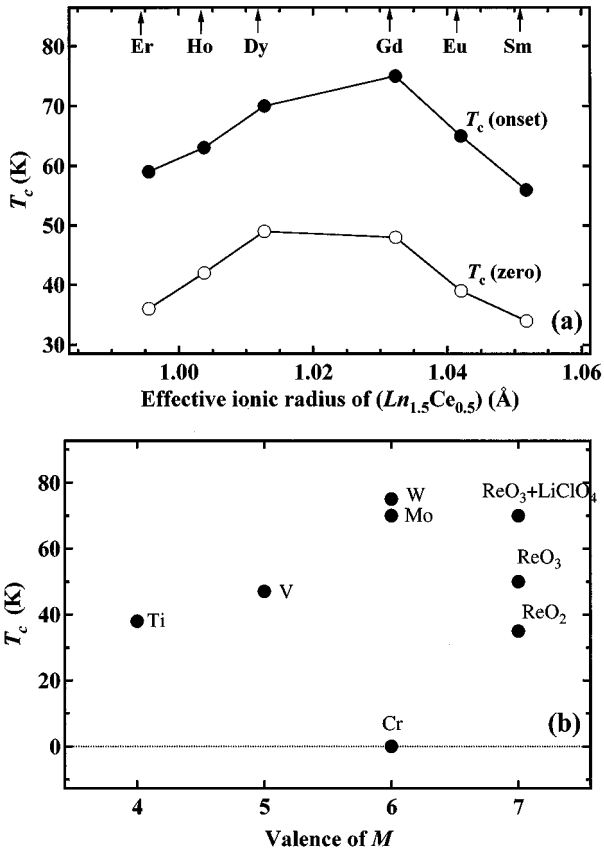

FIG. 7. Variation of T_c with (a) the effective ionic radii of the $(Ln_{1.5}Ce_{0.5})$ site and (b) the valences of the M element in the composition $(Hg_{0.75}M_{0.25})Sr_2(Ln_{1.5}Ce_{0.5})Cu_2O_z$.

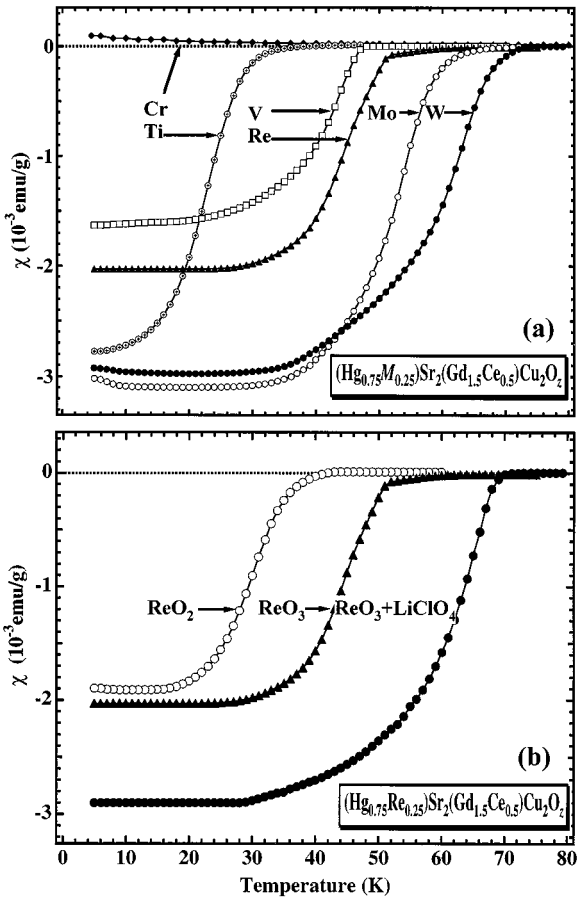

FIG. 8. Temperature dependence of magnetic susceptibility for $(Hg_{0.75}M_{0.25})Sr_2(Gd_{1.5}Ce_{0.5})Cu_2O_z$ (a) M = Ti, V, Cr, Mo, W, and Re and (b) M = Re measured in field-cooling conditions in an external field of 20 Oe.

Cr)-1201 phase, (Hg, Cr)Sr_2CuO_z, exhibits superconductivity with T_c as high as 60 K (10), whereas, the corresponding (Hg, Cr)-1212 phase, (Hg, Cr)Sr_2(Ca, Y)Cu_2O_z, was reported to be nonsuperconducting (16), owing to the carrier-underdoped state caused by the electron doping effect of the yttrium substitution for Ca. Recently, we were able to observe superconductivity at 80 K in yttrium-free (Hg, Cr)-1212, (Hg, Cr)$Sr_2CaCu_2O_z$ synthesized under 6 GPa (37).

TABLE 4
Structural and Superconducting Properties of the Series $(Hg_{0.75}M_{0.25})Sr_2(Gd_{1.5}Ce_{0.5})Cu_2O_z$

M	a (Å)	c (Å)	T_c (K)	Volume fraction (%)
Ti	3.8426(4)	29.229(5)	38	20
V	3.8566(9)	29.126(7)	47	11
Cr	3.8573(7)	29.122(6)	—	—
Mo	3.8420(1)	29.209(8)	70	21
W	3.8327(7)	29.150(6)	75	21
Re[a]	3.8466(4)	29.158(3)	39	14
Re[b]	3.8455(6)	29.140(4)	50	15
Re[c]	3.8437(2)	29.131(3)	70	22

[a] *Re*O_2 is used as *Re* source.
[b] *Re*O_3 is used as *Re* source.
[c] *Re*O_3 and 10% LiClO$_4$ are used.

The maximum T_c obtained in this study is 75 K for the composition $(Hg_{0.75}W_{0.25})Sr_2(Gd_{1.5}Ce_{0.5})Cu_2O_z$. This T_c value is much higher than those (= 10–50 K) observed for the other 1222 phases reported earlier (10–50 K) which were synthesized under ambient or high pressures. However, it is still too low compared with that (= 100 K) reported for (Hg, M)-1212, (Hg, M)$Sr_2(Ln, Ca)Cu_2O_z$, and other phases having two CuO_2 sheets interleaved by a single fluorite layer. This difference may arise from the fact that the CuO_2 sheets in the former are more widely separated (intersheet distance of $\sim$6 Å) than in the latter ones (intersheet distance of $\sim$3.3 Å). The wide distance between the CuO_2 sheets in the double fluorite phase may lead to a weaker coupling between the CuO_2 sheets which is reflected in the lower value of T_c. This argument is strongly supported by the fact that the T_cs of 40–75 K observed in the present study for (Hg,

M)Sr_2(Ln, Ce)$_2Cu_2O_z$ are close to those of a single CuO_2 layered cuprates, i.e., (Hg, M)-1201, (Hg, M)Sr_2CuO_z (10, 17, 38).

CONCLUSION

We have systematically synthesized (Hg, M)Sr_2(Ln, Ce)$_2$ Cu_2O_z (M = Ti, V, Cr, Mo, W, Re, and Ln = Sm, Eu, Gd, Dy, Ho, Er) with (Hg, M)-1222 structure under 2 GPa. Except M = Cr, all the samples show bulk superconductivity with fairly large Meissner volume fractions. As we pointed out in the discussions, the T_c value is correlated to the effective ionic radius of the (Ln, Ce) site as well as the value of the valences of M elements. The maximum T_c (= 75 K) is observed by the sample with nominal composition $(Hg_{.075}W_{0.25})Sr_2(Gd_{1.5}Ce_{0.5})Cu_2O_z$. It is the highest T_c yet observed for 1222-type compound. However, it is still low, compared with that (T_c = 100 K) reported for (Hg, M)Sr_2(Ln, Ca)Cu_2O_z. It seems that the fluorite-type slab is unfavorable for superconductivity in comparison with the (Ln, Ca) layer.

ACKNOWLEDGMENT

This work was supported by the New Energy and Industrial Technology Development Organization (NEDO) as Collaborative Research and Development of Fundamental Technologies for Superconductivity Applications under the New Sunshine Program administered by the Agency of Industrial Science and Technology (AIST) of the Ministry of International Trade and Industry (MITI) of Japan.

REFERENCES

1. S. N. Putilin, E. V. Antipov, O. Chmaissem, and M. Marezio, *Nature* (*London*) **362,** 226 (1993).
2. V. A. Alyoshin, D. A. Mikhailova, and E. V. Antipov, *Physica C* **271,** 197 (1996).
3. S. M. Loureiro, E. V. Antipov, J. L. Tholence, J. J. Capponi, O. Chmassiem, Q. Huang, and M. Marezio, *Physica C* **217,** 253 (1993).
4. M. Paranthaman, *Physica C* **222,** 7 (1994).
5. B. A. Scotte, E. Y. Suard, C. C. Tsuei, D. B. Mitzi, T. R. Mcguire, B. H. Chen, and D. Walker, *Physica C* **230,** 239 (1994).
6. A. Maignan, D. Pelloquin, S. Malo, C. Michel, M. Hervieu, and B. Raveau, *Physica C* **243,** 233 (1995).
7. J. Shimoyama, K. Kishio, S. Hahakura, K. Kitazawa, K. Yamaura, Z. Hiroi, and M. Takano, "Advances in Superconductivity: Proceedings, 7th International Symposium on Superconductivity (ISS'97)," vol. 7, pp. 287. 1997.
8. P. V. P. S. S. Sastry, K. M. Amm, D. C. Knoll, S. C. Peterson, Ch. Wolters, and J. Schwartz, *J. Supercond.* **11,** 49 (1998).
9. P. V. P. S. S. Sastry, K. M. Amm, D. C. Knoll, S. C. Peterson, and J. Schwartz, *Physica C* **297,** 223 (1998).
10. J. Shimoyama, S. Hahakura, K. Kitazawa, K. Yamafuji, and K. Kishio, *Physica C* **224,** 1 (1994).
11. S. Hahakura, J. Shimoyama, O. Shiino, and K. Kishio, *Physica C* **233,** 1 (1994).
12. K. Tang, Y. Qian, Z. Chen, L. Yang, L. Wang, and Y. Zhang, *Physica C* **242,** 216 (1995).
13. R. S. Liu, S. F. Hu, D. A. Jefferson, P. P. Edwards, and P. D. Hunneyball, *Physica C* **205,** 206 (1993).
14. D. Pelloquin, M. Hervieu, C. Michel, G. Van Tendeloo, A. Maignan, and B. Raveau, *Physica C* **216,** 257 (1993).
15. S. F. Hu, D. A. Jefferson, R. S. Liu, and P. P. Edwards, *J. Solid State Chem.* **103,** 280 (1993).
16. O. Chmaissem and Z. Z. Sheng, *Physica C* **242,** 2 (1995) 3.
17. K. Tang, X. Xu, Y. Qian, Z. Chen, L. Yang, and Y. Zhang, *Physica C* **255,** 188 (1995).
18. K. Tang, Y. Qian, Z. Chen, and Y. Zhang, *J. Superconduct.* **9,** 93 (1996).
19. E. Kandyel, T. Kamiyama, H. Asano, S. Amer, and M. Abou-Sekkina, *Jpn. J. Appl. Phys.* **36,** L6306 (1997).
20. E. Kandyel, T. Kamiyama, H. Asano, and M. Abou-Sekkina, *Physica C* **291,** 97 (1997).
21. G. Van Tendeloo, M. Hervieu, X. F. Zhang, and B. Raveau, *J. Solid State Chem.* **114,** 369 (1995); A. Maignan, C. Martin, C. Michel, M. Hervieu, and B. Raveau, *J. Solid State Chem.* **115,** 525 (1995).
22. K. Tang, X. Xu, Y. Qian, Z. Chen, L. Yang, and Y. Zhang, *Physica C* **249,** 1 (1995).
23. J. Akimitsu, S. Suzuki, M. Watanabe, and H. Sawa, *Jpn. J. Appl. Phys.* **27,** L1859 (1988).
24. H. Sawa, S. Suzuki, M. Watanabe, J. Akimitsui, H. Matsubara, H. Watabe, S. Uchida, K. Kousho, H. Asano, F. Izumi, and E. Takayama-Muromachi, *Nature* (*London*) **337,** 347 (1989).
25. Y. Tokura, H. Takagi, and S. Uchida, *Nature* (*London*) **337,** 345 (1989).
26. H. Sawa, K. Obara, J. Akimitsui, Y. Matusi, and S. Horiuchi, *J. Phys. Soc. Jpn.* **58,** 2252 (1989).
27. A. Ichinose, T. Wada, Y. Yaegashi, H. Yamauchi, and S. Tanaka, *Jpn. J. Appl. Phys.* **28,** L1765 (1989); *Jpn. J. Appl. Phys.* **28,** L1779 (1989); *Jpn. J. Appl. Phys.* **29,** L266 (1990).
28. T. Maeda, K. Sakuyama, S. Koriyama, A. Ichinose, H. Yamauchi, and S. Tanaka, *Physica C* **169,** 133 (1990).
29. T. Maeda, K. Sakuyama, N. Sakai, H. Yamauchi, and S. Tanaka, *Physica C* **177,** 337 (1991).
30. N. Sakai, T. Maeda, H. Yamaguchi, and S. Tanaka, *Physica C* **212,** 75 (1993).
31. F. Izumi, *in* 'The Rietveld Method" (R. A. Young, Ed.), Chap. 13, Oxford Univ. Press, Oxford, 1993; Y.-I. Kim and F. Izumi, *J. Ceram. Soc. Jpn.* **102,** 401 (1994).
32. R. D. Shannon, *Acta Crystallogr. A* **32,** 751 (1976).
33. T. Wada, A. Ichinose, F. Izumi, A. Nara, H. Yamauchi, H. Asano, and S. Tanaka, *Physica C* **179,** 445 (1991).
34. O. Chmaissem, D. N. Argyriou, D. G. Hinks, J. D. Jorgensen, B. G. Storey, H. Zhang, L. D. Marks, Y. Y. Wang, V. P. Dravid, and B. Dabrowski, *Phys. Rev. B* **52,** 15 635 (1995).
35. O. Chmaissem, J. D. Jorgensen, D. G. Hinks, B. G. Storey, B. Dabrowski, H. Zhang, and L. D. Marks, *Physica C* **279,** 1 (1997).
36. O. Chmaissem, J. D. Jorgensen, K. Yamura, Z. Hiroi, M. Takano, J. Shimoyama, and K. Kishio, *Phys. Rev. B* **53,** 14647 (1996).
37. E. Kandyel, X.-J. Wu, S. Adachi, and S. Tajima, *Physica C* **322,** 9 (1999).
38. J. B. Mandal, B. Bandyopadhyay, F. Fauth, T. Chattopadhyay, and B. Ghosh, *Physica C* **264,** 145 (1996).